ChemPubSoc Europe

DOI: 10.1002/cptc.201900256

CHEMPHOTOCHEM Articles

Insights into the Optical Properties of Triarylboranes with Strongly Electron-Accepting Bis(fluoromesityl)boryl Groups: when Theory Meets Experiment

Houmam Belaidi,[a] Florian Rauch,[b] Zuolun Zhang,[b, c] Camille Latouche,*[d] Abdou Boucekkine,*[a] Todd B. Marder,*[b] and Jean-François Halet*[a]

The photophysical properties (absorption, fluorescence and phosphorescence) of a series of triarylboranes of the form 4-D–C_6H_4–B(Ar)$_2$ (D = ^{t}Bu or NPh_2; Ar = mesityl (Mes) or 2,4,6-tris (trifluoromethylphenyl (Fmes)) were analyzed theoretically using state-of-the-art DFT and TD-DFT methods. Simulated emission spectra and computed decay rate constants are in very good agreement with the experimental data. Unrestricted electronic computations including vibronic contributions explain the unusual optical behavior of 4-^{t}Bu–C_6H_4–B(Fmes)$_2$ **2**, which shows both fluorescence and phosphorescence at nearly identical energies (at 77 K in a frozen glass). Analysis of the main normal modes responsible for the phosphorescence vibrational fine structure indicates that the bulky *tert*-butyl group tethered to the phenyl ring is strongly involved. Interestingly, in THF solvent, the computed energies of the singlet and triplet excited states are very similar for compound **2** only, which may explain why **2** shows phosphorescence in contrast to the other members of the series.

1. Introduction

A large number of air-stable conjugated three-coordinate organoboron compounds have been synthesized over the last few decades[1–8] for various applications, particularly in linear[9–24] and nonlinear[25–39] optics, electro-optic devices,[40–42] anion sensors,[43,44] cell imaging,[45–48] etc. The boron center in these species possesses an empty *p*-orbital and can thus serve as a strong π-acceptor following photo-excitation, or as a readily reducible center.

Due to their high Lewis acidity, these compounds need to be protected from nucleophilic attack. The most prominent strategies are to shield the boron center using sterically-demanding *ortho*-substituents, or to force a triarylborane into planarity via structural constraints.[11,49–56] In sterically shielded systems, mesityl and larger 1,3,5-trialkylphenyl groups are typically employed as bulky substituents on boron to achieve stability with respect to hydrolysis or other nucleophilic attack at the Lewis acidic boron center. Alternative bulky groups with higher electron affinities should enhance acceptor strength while maintaining or even enhancing the desired chemical stability of the systems.[6,12,28,36–38,57–67] Exploiting this favorable property, some of us recently reported a series of air-stable bis (fluoromesityl)boryl ((FMes)$_2$B) derivatives, namely compounds **1**–**3** (Scheme 1) with different electron-donating groups for comparison, i.e., phenyl, 4-tert-butylphenyl and 4-N,N-diphenylaminophenyl, respectively, attached to the electron acceptor group (FMes)$_2$B through B–C bonds.[12] Comparison of these (FMes)$_2$B-containing donor-acceptor compounds with compound **4**, which contains a (Mes)$_2$B group (Scheme 1), confirms that (FMes)$_2$B is a much stronger acceptor, leading to: (i) a larger quinoidal distortion in the ground state structure; (ii)

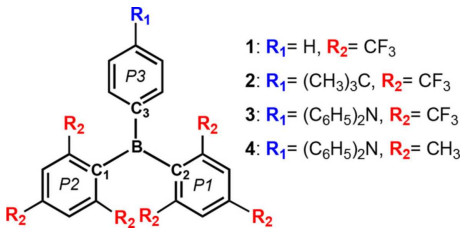

Scheme 1. Molecular structures of compounds **1**–**4**. The two 2,4,6-substituted aryl rings are labelled *P1* and *P2*, and the remaining ring is labelled *P3*. Hydrogen atoms were omitted for clarity.

[a] *Dr. H. Belaidi, Prof. Dr. A. Boucekkine, Prof. Dr. J.-F. Halet*
Univ Rennes, CNRS
Institut des Sciences Chimiques de Rennes
UMR 6226, 35000 Rennes (France)
E-mail: aboucekk@univ-rennes1.fr
halet@univ-rennes1.fr
[b] *F. Rauch, Prof. Dr. Z. Zhang, Prof. Dr. T. B. Marder*
Institut für Anorganische Chemie and Institute for Sustainable Chemistry & Catalysis with Boron
Julius-Maximilians-Universität Würzburg
Am Hubland, 97074 Würzburg (Germany)
E-mail: todd.marder@uni-wuerzburg.de
[c] *Prof. Dr. Z. Zhang*
State Key Laboratory of Supramolecular Structure and Materials
College of Chemistry
Jilin University
Qianjin Street, Changchun (P. R. China)
[d] *Dr. C. Latouche*
Institut des Matériaux Jean Rouxel
Université de Nantes, CNRS
2 rue de la Houssinière, BP 32229
44322 Nantes cedex 3 (France)
E-mail: camille.latouche@univ-nantes.fr

Supporting information for this article is available on the WWW under https://doi.org/10.1002/cptc.201900256

significantly red-shifted emission in solution and in the solid state; (iii) stronger emission solvatochromism; and (iv) significantly lower reduction potentials.[12]

A combination of photophysical measurements and density-functional theory (DFT) computations indicated that the excited states of **2** and **3** relax from the Franck-Condon geometry to a twisted intramolecular charge transfer (TICT) excited state. For comparison, a much smaller structural reorganization prior to emission is expected for compound **4**. Interestingly, the emission spectrum of **2** at 77 K in a 2-MeTHF frozen glass contains a significant phosphorescence contribution arising from an extremely long-lived ($\tau = 2.47$ s) triplet excited state, which is superimposed on the expected fluorescence emission (i.e., both occur at very similar energies).[12] We wondered what makes compound **2** so unusual, and why is it different from compounds **1**, **3**, and **4** with respect to its photophysical properties?

When experiments fail to give a straight answer to a question, it is tempting nowadays to ask whether theory can help to providing an explanation. Indeed, this paper reports state-of-the-art density functional theory (DFT) computations which offer additional insight into the optical and electronic properties of compounds **1**–**4**. Fluorescence spectra, decay rate constants and phosphorescence spectra were simulated and compared with experimental data. The outstanding agreement observed between theory and experiment demonstrates that our theoretical approach represents a particularly reliable and efficient method by which to investigate the optical properties of complex systems.

Computational Details

Calculations were performed at the DFT level with the Gaussian 09 package,[68] using the CAM-B3LYP[69] functional and the 6-31G* basis set. Solvent effects were simulated using the Polarizable Continuum Model (PCM).[70,71] Dispersion effects were taken into account using Grimme's empirical dispersion with Becke-Johnson damping (GD3BJ).[72,73] The nature of the stationary points after optimization of the ground state (S_0) geometries were examined by calculations of the harmonic vibrational frequencies of the respective compounds. Optimizations of the first singlet excited state, hereafter labeled S_1, were performed using the TD-DFT approach. In order to simulate the phosphorescence spectra of **2**, optimization and vibrational frequency calculations of the first triplet excited state, hereafter labeled T_0, were carried out using the unrestricted method. Simulation of the optical spectra was obtained using the VMS software.[74] The phosphorescence spectrum of **2** was simulated including vibronic coupling within the Adiabatic Hessian (AH) model. This model, which explicitly includes mode-mixing between fundamental and excited states, reproduces accurately the optical properties of molecular systems.[75–80] To ensure a sufficient spectrum progression (>90%), normal modes with the lowest energies were neglected in the vibronic treatment. Molecular orbitals (MO) were visualized with the GaussView package.[81]

2. Results and Discussion

2.1. Ground-State Molecular Structures

The ground state geometries of compounds **2**–**4** were first optimized at the CAM-B3LYP/6-31G* level in the gas phase and in hexane solution. Pertinent calculated bond lengths and angles are given in Table 1 and are compared with their corresponding crystallographically measured values.[12] An excellent agreement is observed between theory and experiment, with deviations not larger than a few thousandths of an Å for the distances and less than a few degrees for the bond and dihedral angles. Note that the geometries optimized at the CAM-B3LYP/6-31G* level differ very slightly from those com-

Table 1. Pertinent computed bond lengths [Å], bond angles [°], and dihedral angles [°] for compounds **2**–**4**. See Scheme 1 for the atom labeling.

2 Bond lengths	X-ray[12]	$S_{0\,gas}$	$S_{0\,hexane}$
B–C_1	1.606(3)	1.599	1.599
B–C_2	1.607(3)	1.599	1.600
B–C_3	1.546(3)	1.540	1.540
Bond angles			
C_1–B–C_2	125.7(2)	122.4	122.4
C_1–B–C_3	119.2(2)	118.8	118.7
C_2–B–C_3	115.2(2)	118.9	118.9
Dihedral angles			
P1–BC3 plane	53.17(7)	51.3	51.4
P2–BC3 plane	50.44(7)	51.0	51.0
P3–BC3 plane	29.19(7)	28.4	28.4
3 Bond lengths	X-ray[12]	$S_{0\,gas}$	$S_{0\,hexane}$
B–C_1	1.596(7)/1.605(7)	1.600	1.600
B–C_2	1.612(7)/1.595(7)	1.599	1.600
B–C_3	1.534(7)/1.541(7)	1.530	1.530
Bond angles			
C_1–B–C_2	127.9(4)/127.1(4)	122.6	122.6
C_1–B–C_3	115.8(4)/115.7(4)	118.6	118.6
C_2–B–C_3	116.2(4)/117.2(4)	118.8	118.8
Dihedral angles			
P1–BC3 plane	52.3(2)/50.6(2)	51.1	51.2
P2–BC3 plane	66.2(2)/65.2(2)	51.0	51.0
P3–BC3 plane	26.9(2) /25.4(2)	28.1	27.9
4 Bond lengths	X-ray[12]	$S_{0\,gas}$	$S_{0\,hexane}$
B–C_1	1.579(2)	1.575	1.576
B–C_2	1.583(2)	1.575	1.576
B–C_3	1.561(2)	1.551	1.550
Bond angles			
C_1–B–C_2	123.8(1)	121.6	121.6
C_1–B–C_3	116.6(1)	119.2	119.2
C_2–B–C_3	119.6(1)	119.2	119.2
Dihedral angles			
P1–BC3 plane	52.59(5)	55.2	55.5
P2–BC3 plane	56.60(5)	55.2	55.5
P3–BC3 plane	19.47(5)	22.7	22.3

puted previously at the B3LYP/6-31G* level.[12] Trigonal planar boron atoms are observed in all compounds. Interestingly, geometries computed in the gas phase and in hexane solution are nearly identical.

The electronic structures of compounds **2**–**4** were then analyzed.[12] For compound **2**, for example, the HOMO and HOMO-1, quite energetically separated from the rest of the occupied MOs, are π-type in character and are localized on the 4-*tert*-butylphenyl moiety (Figure 1). The energetically isolated LUMO, also of π-type, is mainly localized on the boron atom.

2.2. Absorption Properties

TD-DFT computations were carried out at the CAM-B3LYP/6-31G* level using the optimized ground state geometries to simulate the optical absorption spectra of molecules **2**–**4** in hexane. Overall, the results agree satisfactorily with experimental data and with the previously computed ones (Table 2).[12]

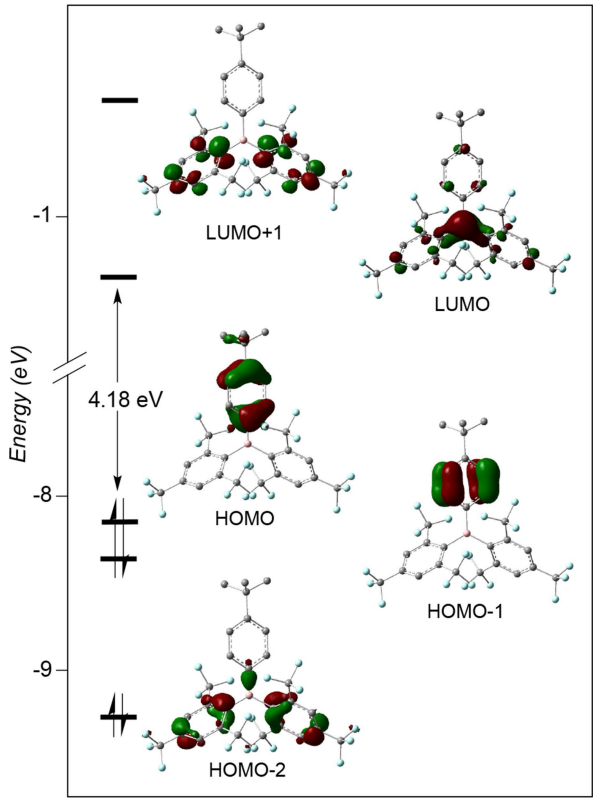

Figure 1. Frontier molecular orbital diagram of **2** (contour values are ±0.06 (e/bohr^3)$^{1/2}$). Hydrogen atoms were omitted for clarity.

For all compounds, the lowest energy absorption corresponds to an electronic excitation from the HOMO to the LUMO. In the case of **2**, for example, it involves a charge transfer (CT) from the 4-*tert*-butylphenyl moiety to the boron-based π-type accepting MO (mostly boron-p_z). As can be seen in Figure 2, solvent effects hardly influence the energy and the intensity of the simulated lowest energy absorption band, which occurs at ca. 290 nm in all cases (Table 3).

2.3. Emission – Fluorescence

Let us focus now on the emission spectra of **2**–**4**. The fluorescence is discussed first. The fluorescence emission wavelengths were computed by optimizing the first singlet excited state using TD-DFT computations. Note that with the aforementioned level of theory, i.e., full CAM-B3LYP computations, the energy agreement with experiment is somewhat better than that of the previously reported theoretical calculations (Table 4).[12] Indeed, compound **2** shows, experimentally, an emission at 426 nm, which was computed at 449 nm.[12] The methodology used herein gives a value of 432 nm. In the cases of **3** and **4**, we also observe slight improvements. It is noteworthy that the methodology used here shows a satisfac-

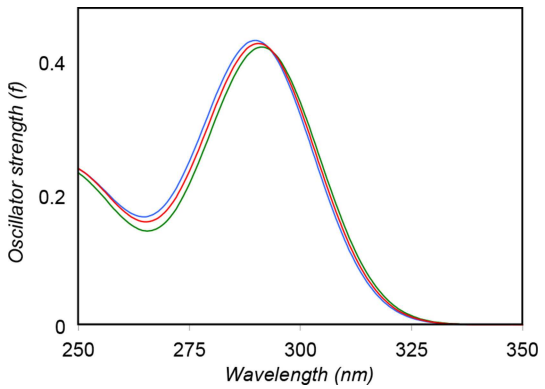

Figure 2. CAM-B3LYP DFT simulated UV-visible absorption spectra of **2** in the gas phase (blue), hexane (green) and THF (red).

Table 3. Experimental (λ_{abs}, nm, eV in parentheses) and computed (λ_{calc}, nm, eV in parentheses) absorption properties of **2**.

Solvent	λ_{abs}	λ_{calc}	f[a]	Transition
Gas	–	290 (4.28)	0.41	HOMO→LUMO
Hexane	318 (3.90)	291 (4.26)	0.40	(>90%)
THF	317 (3.91)	292 (4.25)	0.41	

[a] Oscillator strength.

Table 2. Experimental and computed absorption wavelengths (nm, eV in brackets) of compounds **2**–**4** in hexane.[12]

Cmpd.	**2**	**3**	**4**
Exp.[12]	318 (3.90)	444 (2.79)	377 (3.29)
Calcd.[12]	293 (4.23)	369 (3.36)	330 (3.76)
Calcd.	291 (4.26)	377 (3.29)	334 (3.71)

Table 4. Experimental and computed fluorescence wavelengths (λ_{em}, nm, eV in parentheses) in hexane, for **2**–**4**.

Cmpd.	**2**	**3**	**4**
Exp.[12]	426 (2.91)	563 (2.20)	410 (3.02)
Calcd.[12]	449 (2.76)	579 (2.14)	361 (3.43)
Calcd.	432 (2.87)	547 (2.27)	367 (3.38)

tory reproduction of the emission wavelengths measured experimentally in all regions of the UV-visible spectrum (violet-blue for compounds **2** and **4**, green-yellow for compound **3**).

Overall, the average deviation between the experimental spectra and the simulated fluorescence emissions is ca. 0.15 eV. It should be mentioned that the computed electronic Stokes shifts (peak to peak), ~11000, ~8000 and ~2500 cm^{-1} for **2**, **3**, and **4**, respectively, compare rather well with the experimental data at room temperature which are 8000, 4800 and 2100 cm^{-1} in hexane, respectively.[12]

2.4. Radiative Decays and Fluorescence Lifetimes

To assess fully the validity of our computational approach to investigate molecular excited states, the radiative decay rates together with the fluorescence lifetimes were computed and compared with the available experimental data. To do that, the following equation [Eq. (1)][82] was used:

$$k_r = \frac{4}{3}\left(\frac{\Delta E_{10}}{c}\right)^3 {\mu_{10}}^2 \quad (1)$$

where all the terms are expressed in atomic units (au); ${\mu_{10}}^2$ corresponds to the transition dipole moment strength, ΔE_{10} is the transition energy between S_1 and S_0, i.e., the fluorescence wavelength (in au), and c is approximated to be 137.04 au (1 au ~2.4×10^{-17} seconds). The results are gathered in Table 5.

Interestingly, the computed decay rates of **2**, **3** and **4** are in agreement with the experimental decay rates: (i) the trend is fully reproduced, especially the one order of magnitude difference between **4** and the two other compounds; and (ii) the observed factor of two between **2** and **3** is also well reproduced.

Fluorescence lifetimes τ_r, computed from the k_r equation given above, reproduce relatively well those observed experimentally, decreasing upon going from **2** to **3** to **4** (Table 5). It should also be pointed out that the experimentally measured fluorescence lifetimes take into account non-radiative decay processes, which are not computed here. Experimentally, the value of the non-radiative decay rate constant is larger than that of the radiative decay rate constant for **2** and **3**.[12] This fully explains the very good agreement between τ_r (simulated) and τ (experimental) for **4**, which has a fluorescence quantum yield (Φ_F) in hexane of 0.61, and the moderate agreement for **2** ($\Phi_F = 0.27$) and **3** ($\Phi_F = 0.34$). If one only takes the radiative decay for **2** and **3**, the observed radiative lifetime would be 34.5 and 17.9 ns, respectively. As a consequence, non-radiative processes are slightly more efficient than the radiative ones, explaining the relatively short fluorescence lifetimes observed for these compounds.

Table 5. Relevant computed and experimental (in hexane) photophysical data for **2**–**4**.

Cmpd.	2	3	4
λ_{10} [nm]	432	547	367
ΔE_{10} [au]	0.105	0.083	0.124
$\lvert\mu_{10}\rvert^2$ [au]	0.457	1.47	8.69
$k_r$calc. [au]	2.8×10^{-10}	4.4×10^{-10}	8.6×10^{-9}
$k_r$calc.$[s^{-1}]$	1.2×10^{7}	1.8×10^{7}	3.6×10^{8}
$k_r$exp.$[s^{-1}]$	2.9×10^{7}	5.6×10^{7}	2.6×10^{8}
τ_r-calc. [ns]	87.00	55.10	2.81
τ_r-exp. [ns]	34.00	17.90	3.80
τ-exp. [ns]	9.30	6.12	2.40

2.5. Emission – Phosphorescence

The main question is why, in contrast to **3** and **4**, does **2** also show phosphorescence at low temperature in 2-MeTHF (77 K, frozen glass).[12] On this basis, an investigation of the first triplet excited state (T_0) was attempted for **2**. It turns out that the luminescence spectrum of **2** is indeed the sum of both fluorescence and phosphorescence components. Therefore, T_0 and S_1 were both investigated (computations were conducted with THF to simulate 2-MeTHF).

The computed fluorescence emission (in THF) occurs at around 400 nm and fits nicely with the experimental value (~400 nm)[12] Experimentally, the phosphorescence spectrum exhibits a first emission band around 420 nm, a second band at *ca.* 450 nm and a shoulder just above 475 nm.[12] The first triplet excited state (T_0, unrestricted) of **2** was computed. The optimized geometry was shown to be a true energy minimum on the potential energy surface by diagonalization of the Hessian matrix (frequency calculations). The computed phosphorescence wavelength, obtained from the energy difference between T_0 and S_0 is 412 nm, in a very good agreement with the first emission band observed experimentally at 420 nm.

In order to simulate the shape of the phosphorescence spectrum, the adiabatic Hessian (AH) approach was used (see computational details). In this method, computation of the normal modes of vibration for the geometry-optimized S_0 and T_0 states is necessary. Note that such a model is valid only if the geometries of the initial (S_0) and final (T_0) states are rather similar.[83,84] Interestingly, the geometries of S_0 and T_0 of **2** are computed to be rather similar (Table 6 and Figure 3, right)

Table 6. Pertinent computed bond lengths [Å] and bond and dihedral angles [°] of the S_0, S_1, and T_0 states of compound **2** in THF solvent. See Scheme 1 for the atom labeling.

	S_0	S_1	T_0
Bond lengths			
B–C_1	1.599	1.604	1.588
B–C_2	1.599	1.535	1.592
B–C_3	1.541	1.572	1.528
Bond angles			
C_1–B–C_3	122.5	126.7	123.0
C_2–B–C_3	118.8	109.4	118.2
C_2–B–C_3	118.7	123.9	118.8
Dihedral angles			
P1–BC3 plane	51.4	63.3	50.9
P2–BC3 plane	51.0	29.6	51.5
P3–BC3 plane	28.5	67.0	25.1

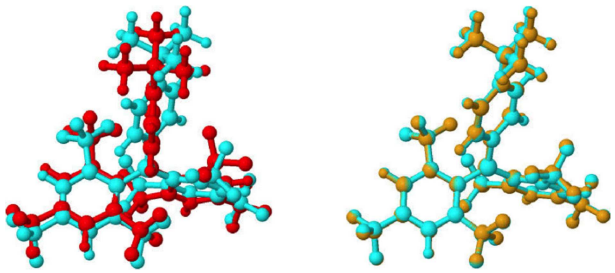

Figure 3. Superimposed S_0 (cyan)/S_1 (red; left) and S_0 (cyan)/T_0 (yellow; right) state geometries of **2**.

leading to a good overlap between the normal modes of the ground and excited states. It was thus possible to simulate the phosphorescence spectrum using the AH model. On the other hand, there is a greater degree of structural distortion when going from S_0 to S_1 (Table 6 and Figure 3, left). This explains why the AH model of vibronic coupling cannot be used to simulate the fluorescence spectrum properly. As our results regarding the fluorescence are sufficient to explain the optical properties of compound **2** (see above), we think that such a simulation is not necessary here. Note that geometry changes between S_0, S_1, and T_0 are more important for compounds **3** and **4** (see Table S1, Supporting Information).

As depicted in Figure 4, the simulated phosphorescence spectrum of **2** nicely matches the experimental one[12] (it is shifted by ~0.04 eV in order to superimpose its maximum with that of the experimental one). Note that in order to reach a sufficient spectrum convergence (>90%), normal modes smaller than 100 cm^{-1} were excluded from the vibronic calculations. Indeed, both the position and intensity of the bands are well reproduced. A sharp peak at 420 nm is observed both theoretically and experimentally. The broad band experimentally measured around 450 nm corresponds to two small computed bands. The shoulder occurring at *ca.* 475 nm consists of three peaks in our simulation.

The excellent match between the simulated and the observed spectra allows us to assign the vibrational normal modes contributing to the phosphorescence phenomenon of **2**. This was carried out using the computed shift-vectors (i.e., using the gradient of the final state projected onto the normal modes of the initial state).[85]

The most important contributing vibrational modes 26, 27, 28, 85, 95 and 167 which appear at 165 (164), 168 (167), 182 (202), 712 (734), 857 (879) and 1675 (1701) cm^{-1} at the excited (ground) state, respectively, are shown in Figure 5. Modes 26 and 27 correspond to the torsion of the *tert*-butyl group with respect to the phenyl moiety associated, to a lesser extent, with the wagging and bending of the CF_3 groups. Mode 28 corresponds to the rocking of H atoms of the *tert*-butyl group together with a non-negligible wagging of two CH groups of the phenyl ring. Mode 85 involves the breathing of the whole molecule with a strong scissoring motion of the carbon atoms and some flattening of the CF_3 groups. Mode 95 also shows a strong scissoring motion of the carbon atoms accompanied by some CF_3 stretching and C–B–C torsional motions. Mode 167 can be ascribed mainly to C–C symmetrical stretching and C–H bending in the phenyl ring. One point needs to be clarified. It was mentioned previously that the phosphorescence spectrum of **2** is structured with an average vibrational spacing of ca. 1300 cm^{-1}.[12] This point led to the hypothesis that aromatic ring modes must play a large role in the phosphorescence signature, which is confirmed here. Indeed, according to our simulations, a normal mode with such characteristics occurs at 1337 cm^{-1} with a moderate shift vector and thus may explain the vibrational spacing of ca. 1300 cm^{-1}. This normal mode can

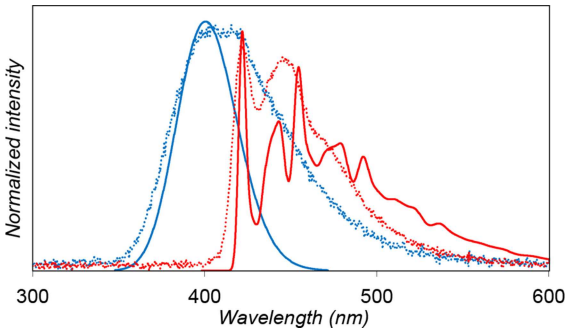

Figure 4. Experimental (dashed) and DFT simulated (solid) fluorescence (blue) and phosphorescence (red) spectra of **2**.

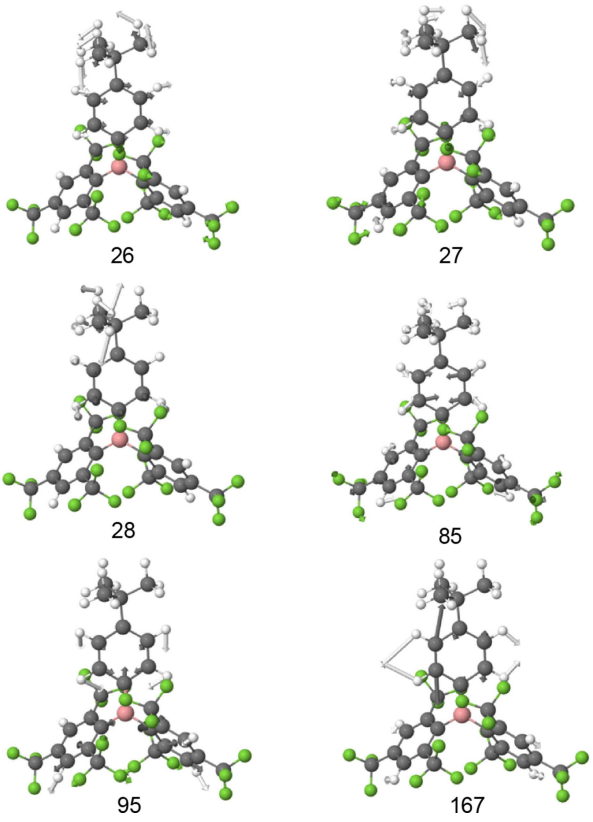

Figure 5. Representation of the normal mode eigenvectors with the largest shift-vector for **2**.

be assigned as a mixture of C–C stretching and C–H bending localized on the Ph–$(CH_3)_3$C moiety.

One of the determining factors regarding the phosphorescent properties of **2** and the fluorescent properties of **3** and **4** at low temperature (77 K, frozen glass) in 2-MeTHF,[12] is the energy difference between the S_1 and T_0 states. As shown in Figure 6, this energy difference is extremely small for **2** (0.01 eV), but rather substantial for **3** (0.34 eV) and **4** (0.61 eV). This might explain why **2** is phosphorescent but not **3** and **4**.

Finally, we wondered why **2** is phosphorescent in 2-MeTHF (frozen glass) but not in hexane, despite the fact that geometries computed at 0 K hardly differ from one solvent to the other (see Table S1 and Figure S1, Supporting Information). Part of the answer resides in the energy difference between S_1 and T_0 which is computed to be very small in THF (0.01 eV) but substantial in hexane (0.60 eV), comparable to those computed for compounds **3** and **4** (see Table 7).

3. Conclusion

In this paper, the photophysical properties of a series of triarylborane derivatives **2**–**4** were theoretically analyzed using state-of-the-art DFT and TD-DFT methods. Simulated fluorescence spectra and computed decay rate constants are in very good agreement with the available experimental data for compounds **2**–**4**. Indeed, the computed orders of magnitude and trends in the radiative decay rate constants fully match those experimentally determined. The unusual optical properties of **2**, which shows both fluorescence and phosphorescence emissions, were investigated. Unrestricted electronic computations coupled with vibronic contributions allowed us to simulate the phosphorescence spectrum of **2** resulting in an outstanding agreement with experimental data. Finally, analysis of the main normal modes responsible of the phosphorescence vibrational fine structure, which were identified using the shift vector protocol, indicates that the bulky *tert*-butyl group tethered to the phenyl ring is strongly involved. In THF solvent, the energies of the singlet and triplet excited states are very close to each other only for compound **2**, which may explain why **2** shows phosphorescence at 77 K in contrast to **3** and **4**. Finally, D-π-A triarylboranes with small singlet-triplet gaps are already proving useful in thermally activated delayed fluorescence (TADF) based materials.[42,86–98] The use of trifluoromethylated aryl groups in three coordinate boron compounds for optical applications provides a very efficient tool to fine tune properties. Consequently, it is of the utmost importance to understand the electronic properties of these systems in detail.

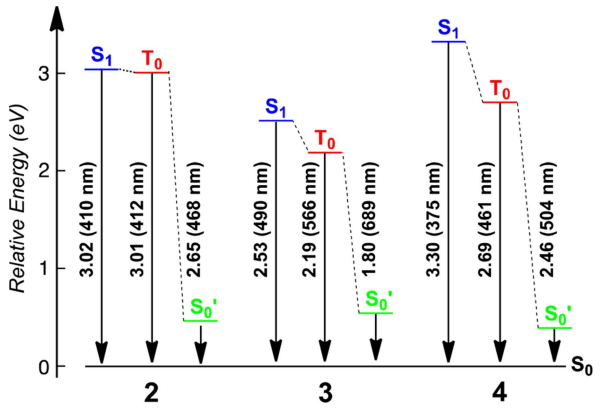

Figure 6. Comparison of the energy of the excited states S_1, T_0 and S_0' for compounds **2**–**4** computed in THF solvent. Vertical emission energies ($T_0 \rightarrow S'_0$) are also given for information.

Table 7. Computed energy difference, $\Delta E = E(S_1) - E(T_0)$ [eV], for compounds **2**–**4** in THF and hexane.

	2	3	4
THF	0.01	0.34	0.61
hexane	0.60	0.59	0.80

Acknowledgements

C.L. thanks the "Centre de Calcul Intensif des Pays de la Loire" (CCIPL) and Région Pays de la Loire to support the "CLIC" project, A.B. and J.-F. H. thank the GENCI-IDRIS and GENCI-CINES (Grant No. 2016-2017-080649) for computational resources. T.B.M. is grateful for generous financial support from the Bavarian State Ministry of Science, Research, and the Arts for the Collaborative Research Network "Solar Technologies go Hybrid" and the DFG (GRK 2112). Z.Z. thanks the Alexander von Humboldt Foundation for a postdoctoral fellowship.

Keywords: boron · density functional calculations · luminescence · phosphorescence · photophysics

[1] L. Ji, S. Griesbeck, T. B. Marder, *Chem. Sci.* **2017**, *8*, 846–863.
[2] C. D. Entwistle, T. B. Marder, *Angew. Chem. Int. Ed.* **2002**, *41*, 2927–2931; *Angew. Chem.* **2002**, *114*, 3051–3056.
[3] C. D. Entwistle, T. B. Marder, *Chem. Mater.* **2004**, *16*, 4574–4585.
[4] Y. Qin, G. Cheng, O. Achara, K. Parab, F. Jäkle, *Macromolecules* **2004**, *37*, 7123–7131.
[5] C.-H. Zhao, A. Wakamiya, Y. Inukai, S. Yamaguchi, *J. Am. Chem. Soc.* **2006**, *128*, 15934–15935.
[6] A. Wakamiya, S. Yamaguchi, *Bull. Chem. Soc. Jpn.* **2015**, *88*, 1357–1377.
[7] G. Turkoglu, M. E. Cinar, T. Ozturk, *Molecules* **2017**, *22*, 1522.
[8] S.-Y. Li, Z.-B. Sun, C.-H. Zhao, *Inorg. Chem.* **2017**, *56*, 8705–8717.
[9] Z. Zhang, R. M. Edkins, J. Nitsch, K. Fucke, A. Eichhorn, A. Steffen, Y. Wang, T. B. Marder, *Chem. Eur. J.* **2015**, *21*, 177–190.
[10] N. Matsumi, K. Naka, Y. Chujo, *J. Am. Chem. Soc.* **1998**, *120*, 5112–5113.
[11] S. Yamaguchi, S. Akiyama, K. Tamao, *J. Am. Chem. Soc.* **2000**, *122*, 6335–6336.
[12] Z. Zhang, R. M. Edkins, J. Nitsch, K. Fucke, A. Steffen, L. E. Longobardi, D. W. Stephan, C. Lambert, T. B. Marder, *Chem. Sci.* **2015**, *6*, 308–321.
[13] J. Merz, J. Fink, A. Friedrich, I. Krummenacher, H. H. Al Mamari, S. Lorenzen, M. Haehnel, A. Eichhorn, M. Moos, M. Holzapfel, H. Braunschweig, C. Lambert, A. Steffen, L. Ji, T. B. Marder, *Chem. Eur. J.* **2017**, *23*, 13164–13180.
[14] W.-L. Jia, D. Song, S. Wang, *J. Org. Chem.* **2003**, *68*, 701–705.
[15] A. Wakamiya, T. Ide, S. Yamaguchi, *J. Am. Chem. Soc.* **2005**, *127*, 14859–14866.
[16] I. Yamaguchi, B.-J. Choi, T. Koizumi, K. Kubota, T. Yamamoto, *Macromolecules* **2007**, *40*, 438–443.

[17] U. Megerle, F. Selmaier, C. Lambert, E. Riedle, S. Lochbrunner, *Phys. Chem. Chem. Phys.* **2008**, *10*, 6245.
[18] A. Lorbach, M. Bolte, H. Li, H.-W. Lerner, M. C. Holthausen, F. Jäkle, M. Wagner, *Angew. Chem. Int. Ed.* **2009**, *48*, 4584–4588; *Angew. Chem.* **2009**, *121*, 4654–4658.
[19] L. Weber, V. Werner, M. A. Fox, T. B. Marder, S. Schwedler, A. Brockhinke, H.-G. Stammler, B. Neumann, *Dalton Trans.* **2009**, 2823–2831.
[20] C. Reus, S. Weidlich, M. Bolte, H.-W. Lerner, M. Wagner, *J. Am. Chem. Soc.* **2013**, *135*, 12892–12907.
[21] X. Yin, J. Chen, R. A. Lalancette, T. B. Marder, F. Jäkle, *Angew. Chem. Int. Ed.* **2014**, *53*, 9761–9765; *Angew. Chem.* **2014**, *126*, 9919–9923.
[22] M. Meier, L. Ji, J. Nitsch, I. Krummenacher, A. Deißenberger, D. Auerhammer, M. Schäfer, T. B. Marder, H. Braunschweig, *Chem. Eur. J.* **2019**, *25*, 4707–4712.
[23] J. Merz, A. Steffen, J. Nitsch, J. Fink, C. B. Schürger, A. Friedrich, I. Krummenacher, H. Braunschweig, M. Moos, D. Mims, C. Lambert, T. B. Marder, *Chem. Sci.* **2019**, *10*, 7516–7534.
[24] X. Jia, J. Nitsch, L. Ji, Z. Wu, A. Friedrich, F. Kerner, M. Moos, C. Lambert, T. B. Marder, *Chem. Eur. J.* **2019**, *25*, 10845–10857.
[25] Z. Yuan, N. J. Taylor, T. B. Marder, I. D. Williams, S. K. Kurtz, L.-T. Cheng, *J. Chem. Soc. Chem. Commun.* **1990**, 1489–1492.
[26] Z. Yuan, N. J. Taylor, Y. Sun, T. B. Marder, I. D. Williams, L.-T. Cheng, *J. Organomet. Chem.* **1993**, *449*, 27–37.
[27] P. Chen, A. S. Marshall, S.-H. Chi, X. Yin, J. W. Perry, F. Jäkle, *Chem. Eur. J.* **2015**, *21*, 18237–18247.
[28] S. Griesbeck, Z. Zhang, M. Gutmann, T. Lühmann, R. M. Edkins, G. Clermont, A. N. Lazar, M. Haehnel, K. Edkins, A. Eichhorn, M. Blanchard-Desce, L. Meinel, T. B. Marder, *Chem. Eur. J.* **2016**, *22*, 14701–14706.
[29] Z. Yuan, N. J. Taylor, R. Ramachandran, T. B. Marder, *Appl. Organomet. Chem.* **1996**, *10*, 305–316.
[30] Z. Liu, Q. Fang, D. Wang, G. Xue, W. Yu, Z. Shao, M. Jiang, *Chem. Commun.* **2002**, 2900–2901.
[31] Z. Liu, Q. Fang, D. Wang, D. Cao, G. Xue, W. Yu, H. Lei, *Chem. Eur. J.* **2003**, *9*, 5074–5084.
[32] M. Charlot, L. Porrès, C. D. Entwistle, A. Beeby, T. B. Marder, M. Blanchard-Desce, *Phys. Chem. Chem. Phys.* **2005**, *7*, 600–606.
[33] Z. Yuan, C. D. Entwistle, J. C. Collings, D. Albesa-Jové, A. S. Batsanov, J. A. K. Howard, N. J. Taylor, H. M. Kaiser, D. E. Kaufmann, S.-Y. Poon, W.-Y. Wong, C. Jardin, S. Fathallah, A. Boucekkine, J.-F. Halet, T. B. Marder, *Chem. Eur. J.* **2006**, *12*, 2758–2771.
[34] C. D. Entwistle, J. C. Collings, A. Steffen, L.-O. Pålsson, A. Beeby, D. Albesa-Jové, J. M. Burke, A. S. Batsanov, J. A. K. Howard, J. A. Mosely, S.-Y. Poon, W.-Y. Wong, F. Ibersiene, S. Fathallah, A. Boucekkine, J.-F. Halet, T. B. Marder, *J. Mater. Chem.* **2009**, *19*, 7532–7544.
[35] J. C. Collings, S.-Y. Poon, C. Le Droumaguet, M. Charlot, C. Katan, L.-O. Pålsson, A. Beeby, J. A. Mosely, H. M. Kaiser, D. Kaufmann, W.-Y. Wong, M. Blanchard-Desce, T. B. Marder, *Chem. Eur. J.* **2009**, *15*, 198–208.
[36] L. Ji, R. M. Edkins, L. J. Sewell, A. Beeby, A. S. Batsanov, K. Fucke, M. Drafz, J. A. K. Howard, O. Moutounet, F. Ibersiene, A. Boucekkine, E. Furet, Z. Liu, J.-F. Halet, C. Katan, T. B. Marder, *Chem. Eur. J.* **2014**, *20*, 13618–13635.
[37] S. Griesbeck, M. Ferger, C. Czernetzi, C. Wang, R. Bertermann, A. Friedrich, M. Haehnel, D. Sieh, M. Taki, S. Yamaguchi, T. B. Marder, *Chem. Eur. J.* **2019**, *25*, 7679–7688.
[38] S. Griesbeck, E. Michail, C. Wang, H. Ogasawara, S. Lorenzen, L. Gerstner, T. Zang, J. Nitsch, Y. Sato, R. Bertermann, M. Taki, C. Lambert, S. Yamaguchi, T. B. Marder, *Chem. Sci.* **2019**, *10*, 5405–5422.
[39] S. Griesbeck, E. Michail, F. Rauch, H. Ogasawara, C. Wang, Y. Sato, R. Edkins, Z. Zhang, M. Taki, C. Lambert, S. Yamaguchi, T. B. Marder, *Chem. Eur. J.* **2019**, *25*, 13164–13175.
[40] Y. Shirota, *J. Mater. Chem.* **2000**, *10*, 1–25.
[41] A. Wakamiya, K. Mori, S. Yamaguchi, *Angew. Chem. Int. Ed.* **2007**, *46*, 4273–4276; *Angew. Chem.* **2007**, *119*, 4351–4354.
[42] K. Suzuki, S. Kubo, K. Shizu, T. Fukushima, A. Wakamiya, Y. Murata, C. Adachi, H. Kaji, *Angew. Chem. Int. Ed.* **2015**, *54*, 15231–15235; *Angew. Chem.* **2015**, *127*, 15446–15450.
[43] S. Yamaguchi, S. Akiyama, K. Tamao, *J. Am. Chem. Soc.* **2001**, *123*, 11372–11375.
[44] T. W. Hudnall, C.-W. Chiu, F. P. Gabbaï, *Acc. Chem. Res.* **2009**, *42*, 388–397.
[45] J. Liu, K. Cheng, C. Yang, J. Zhu, C. Shen, X. Zhang, X. Liu, G. Yang, *Anal. Chem.* **2019**, *91*, 6340–6344.
[46] J. Liu, C. Zhang, J. Dong, J. Zhu, C. Shen, G. Yang, X. Zhang, *RSC Adv.* **2017**, *7*, 14511–14515.
[47] J. Liu, S. Zhang, C. Zhang, J. Dong, C. Shen, J. Zhu, H. Xu, M. Fu, G. Yang, X. Zhang, *Chem. Commun.* **2017**, *53*, 11476–11479.
[48] J. Liu, C. Zhang, J. Dong, J. Zhu, C. Shen, G. Yang, X. Zhang, *New J. Chem.* **2017**, *41*, 4733–4737.
[49] H. C. Brown, V. H. Dodson, *J. Am. Chem. Soc.* **1957**, *79*, 2302–2306.
[50] A. Wakamiya, K. Mishima, K. Ekawa, S. Yamaguchi, *Chem. Commun.* **2008**, 579–581.
[51] S. Saito, K. Matsuo, S. Yamaguchi, *J. Am. Chem. Soc.* **2012**, *134*, 9130–9133.
[52] C. Dou, S. Saito, K. Matsuo, I. Hisaki, S. Yamaguchi, *Angew. Chem. Int. Ed.* **2012**, *51*, 12206–12210; *Angew. Chem.* **2012**, *124*, 12372–12376.
[53] Z. Zhou, A. Wakamiya, T. Kushida, S. Yamaguchi, *J. Am. Chem. Soc.* **2012**, *134*, 4529–4532.
[54] V. M. Hertz, N. Ando, M. Hirai, M. Bolte, H.-W. Lerner, S. Yamaguchi, M. Wagner, *Organometallics* **2017**, *36*, 2512–2519.
[55] Y. Kitamoto, T. Suzuki, Y. Miyata, H. Kita, K. Funaki, S. Oi, *Chem. Commun.* **2016**, *52*, 7098–7101.
[56] X. Yin, F. Guo, R. A. Lalancette, F. Jäkle, *Macromolecules* **2016**, *49*, 537–546.
[57] D.-T. Yang, S. K. Mellerup, J.-B. Peng, X. Wang, Q.-S. Li, S. Wang, *J. Am. Chem. Soc.* **2016**, *138*, 11513–11516.
[58] R. J. Blagg, E. J. Lawrence, K. Resner, V. S. Oganesyan, T. J. Herrington, A. E. Ashley, G. G. Wildgoose, *Dalton Trans.* **2016**, *45*, 6023–6031.
[59] Q. Yan, M. Yin, C. Chen, Y. Zhang, *J. Org. Chem.* **2018**, *83*, 9096–9102.
[60] S. Toyota, M. Asakura, M. Oki, F. Toda, *Bull. Chem. Soc. Jpn.* **2000**, *73*, 2357–2362.
[61] Z. Lu, Z. Cheng, Z. Chen, L. Weng, Z. H. Li, H. Wang, *Angew. Chem. Int. Ed.* **2011**, *50*, 12227–12231; *Angew. Chem.* **2011**, *123*, 12435–12439.
[62] J. Wang, Y. Wang, T. Taniguchi, S. Yamaguchi, S. Irle, *J. Phys. Chem. A* **2012**, *116*, 1151–1158.
[63] Z. Lu, Y. Wang, J. Liu, Y. Lin, Z. H. Li, H. Wang, *Organometallics* **2013**, *32*, 6753–6758.
[64] T. Taniguchi, J. Wang, S. Irle, S. Yamaguchi, *Dalton Trans.* **2013**, *42*, 620–624.
[65] Z. Zhang, R. M. Edkins, M. Haehnel, M. Wehner, A. Eichhorn, L. Mailänder, M. Meier, J. Brand, F. Brede, K. Müller-Buschbaum, H. Braunschweig, T. B. Marder, *Chem. Sci.* **2015**, *6*, 5922–5927.
[66] J. Zheng, Y.-J. Lin, H. Wang, *Dalton Trans.* **2016**, *45*, 6088–6093.
[67] T. E. Stennett, P. Bissinger, S. Griesbeck, S. Ullrich, I. Krummenacher, M. Auth, A. Sperlich, M. Stolte, K. Radacki, C.-J. Yao, F. Würthner, A. Steffen, T. B. Marder, H. Braunschweig, *Angew. Chem. Int. Ed.* **2019**, *58*, 6449–6454; *Angew. Chem.* **2019**, *131*, 6516-6521.
[68] Gaussian 09, revision D01, M. J. Frisch, G. W. Trucks, H. B. Schlegel, G. E. Scuseria, M. A. Robb, J. R. Cheeseman, G. Scalmani, V. Barone, B. Mennucci, G. A. Petersson, H. Nakatsuji, M. Caricato, X. Li, H. P. Hratchian, A. F. Izmaylov, J. Bloino, G. Zheng, J. L. Sonnenberg, M. Hada, M. Ehara, K. Toyota, R. Fukuda, J. Hasegawa, M. Ishida, T. Nakajima, Y. Honda, O. Kitao, H. Nakai, T. Vreven, J. A. Montgomery Jr., J. E. Peralta, F. Ogliaro, M. Bearpark, J. J. Heyd, E. Brothers, K. N. Kudin, V. N. Staroverov, R. Kobayashi, J. Normand, K. Raghavachari, A. Rendell, J. C. Burant, S. S. Iyengar, J. Tomasi, M. Cossi, N. Rega, J. M. Millam, M. Klene, J. E. Knox, J. B. Cross, V. Bakken, C. Adamo, J. Jaramillo, R. Gomperts, R. E. Stratmann, O. Yazyev, A. J. Austin, R. Cammi, C. Pomelli, J. W. Ochterski, R. L. Martin, K. Morokuma, V. G. Zakrzewski, G. A. Voth, P. Salvador, J. J. Dannenberg, S. Dapprich, A. D. Daniels, O. Farkas, J. B. Foresman, J. V Ortiz, J. Cioslowski, D. J. Fox, Gaussian, Inc., Wallingford, CT, USA, **2009**.
[69] T. Yanai, D. P. Tew, N. C. Handy, *Chem. Phys. Lett.* **2004**, *393*, 51–57.
[70] M. Cossi, G. Scalmani, N. Rega, V. Barone, *J. Chem. Phys.* **2002**, *117*, 43–54.
[71] V. Barone, M. Cossi, J. Tomasi, *J. Chem. Phys.* **1997**, *107*, 3210–3221.
[72] S. Grimme, J. Antony, S. Ehrlich, H. Krieg, *J. Chem. Phys.* **2010**, *132*, 094106.
[73] S. Grimme, S. Ehrlich, L. Goerigk, *J. Comput. Chem.* **2011**, *32*, 1456–1465.
[74] D. Licari, A. Baiardi, M. Biczysko, F. Egidi, C. Latouche, V. Barone, *J. Comput. Chem.* **2015**, *36*, 321–334.
[75] V. Barone, J. Bloino, M. Biczysko, F. Santoro, *J. Chem. Theory Comput.* **2009**, *5*, 540–554.
[76] V. Barone, A. Baiardi, M. Biczysko, J. Bloino, C. Cappelli, F. Lipparini, *Phys. Chem. Chem. Phys.* **2012**, *14*, 12404–12422.
[77] H. Ayache, D. Hammoutène, E. Fritsch, A. Elkechai, A. Boucekkine, C. Latouche, *Theor. Chem. Acc.* **2017**, *136*, 108.
[78] F. Massuyeau, E. Faulques, C. Latouche, *J. Chem. Theory Comput.* **2017**, *13*, 1748–1755.

[79] F. Massuyeau, E. Faulques, C. Latouche, V. Barone, *Phys. Chem. Chem. Phys.* **2016**, *18*, 19378–19385.
[80] F. Vazart, C. Latouche, J. Bloino, V. Barone, *Inorg. Chem.* **2015**, *54*, 5588–5595.
[81] J. Dennington, R. Keith, T. Millam, *Gaussview V5* **2009**.
[82] M. Savarese, A. Aliberti, I. De Santo, E. Battista, F. Causa, P. A. Netti, N. Rega, *J. Phys. Chem. A* **2012**, *116*, 7491–7497.
[83] C. Latouche, A. Baiardi, V. Barone, *J. Phys. Chem. B* **2015**, *119*, 7253–7257.
[84] H. Belaidi, S. Belaidi, C. Katan, C. Latouche, A. Boucekkine, *J. Mol. Model.* **2016**, *22*, 265.
[85] F. Egidi, J. Bloino, C. Cappelli, V. Barone, *J. Chem. Theory Comput.* **2014**, *10*, 346–363.
[86] C.-C. Tsai, W.-C. Huang, H.-Y. Chih, Y.-C. Hsh, C.-W. Liao, C.-H. Lin, Y.-X. Kang, C.-H. Chang, Y. J. Chang, C.-W. Lu, *Org. Electron.* **2018**, *63*, 166–174.
[87] T. Hatakeyama, K. Shiren, K. Nakajima, S. Nomura, S. Nakatsuka, K. Kinoshita, J. Ni, Y. Ono, T. Ikuta, *Adv. Mater.* **2016**, *28*, 2777–2781.
[88] M.-Y. Zhang, Z.-Y. Li, B. Lu, Y. Wang, Y.-D. Ma, C.-H. Zhao, *Org. Lett.* **2018**, *20*, 6868–6871.
[89] T.-L. Wu, M.-J. Huang, C.-C. Lin, P.-Y. Huang, T.-Y. Chou, R.-W. Chen-Cheng, H.-W. Lin, R.-S. Liu, C.-H. Cheng, *Nat. Photonics* **2018**, *12*, 235–240.
[90] I. S. Park, K. Matsuo, N. Aizawa, T. Yasuda, *Adv. Funct. Mater.* **2018**, *28*, 1802031.
[91] S.-Y. Li, Z.-B. Sun, C.-H. Zhao, *ACS Omega* **2018**, *3*, 12730–12736.
[92] D.-G. Chen, T.-C. Lin, C.-L. Chen, Y.-T. Chen, Y.-A. Chen, G.-H. Lee, P.-T. Chou, C.-W. Liao, P.-C. Chiu, C.-H. Chang, Y.-J. Lien, Y. Chi, *ACS Appl. Mater. Interfaces* **2018**, *10*, 12886–12896.
[93] C. Tu, W. Liang, *ACS Omega* **2017**, *2*, 3098–3109.
[94] Y.-J. Lien, T.-C. Lin, C.-C. Yang, Y.-C. Chiang, C.-H. Chang, S.-H. Liu, Y.-T. Chen, G.-H. Lee, P.-T. Chou, C.-W. Lu, Y. Chi, *ACS Appl. Mater. Interfaces* **2017**, *9*, 27090–27101.
[95] Y. H. Lee, S. Park, J. Oh, J. W. Shin, J. Jung, S. Yoo, M. H. Lee, *ACS Appl. Mater. Interfaces* **2017**, *9*, 24035–24042.
[96] Y. Kitamoto, T. Namikawa, T. Suzuki, Y. Miyata, H. Kita, T. Sato, S. Oi, *Org. Electron.* **2016**, *34*, 208–217.
[97] M. Numata, T. Yasuda, C. Adachi, *Chem. Commun.* **2015**, *51*, 9443–9446.
[98] Y. Kitamoto, T. Namikawa, D. Ikemizu, Y. Miyata, T. Suzuki, H. Kita, T. Sato, S. Oi, *J. Mater. Chem. C* **2015**, *3*, 9122–9130.

Manuscript received: October 25, 2019
Revised manuscript received: October 31, 2019
Accepted manuscript online: November 10, 2019
Version of record online: December 17, 2019